Journal of Nuclear Materials 515 (2019) 407–419

Contents lists available at ScienceDirect

Journal of Nuclear Materials

journal homepage: www.elsevier.com/locate/jnucmat

Effect of friction stir welding and self-ion irradiation on dispersoid evolution in oxide dispersion strengthened steel MA956 up to 25 dpa

E. Getto [a, *], B. Baker [a], B. Tobie [a], S. Briggs [b, c], K. Hattar [c], K. Knipling [d]

[a] Department of Mechanical Engineering, United States Naval Academy, Annapolis, MD, 21042, USA
[b] School of Nuclear Science and Engineering, Oregon State University, Corvallis, OR, 97331, USA
[c] Sandia National Laboratories, Albuquerque, NM, 87185, USA
[d] Materials Science and Technology Division, United States Naval Research Laboratory, Code 6355, Washington, DC, 20375, USA

HIGHLIGHTS

- Oxide dispersion strengthened alloy MA956 was friction stir welded and irradiated.
- Coarsening of Y–Al–O dispersoids observed with welding and irradiation at 450 °C.
- Potential re-precipitation of dispersoids in welded and irradiated MA956.
- Dislocation loops form early with stable microstructure up to 25 dpa.

ARTICLE INFO

Article history:
Received 27 August 2018
Received in revised form
9 November 2018
Accepted 23 December 2018
Available online 24 December 2018

Keywords:
Oxide dispersion strengthened alloy
MA956
Ion irradiation
Friction stir welding
Microstructure evolution

ABSTRACT

The effect of ion irradiation on the microstructure of oxide dispersion strengthened (ODS) MA956 steel, before and after friction stir welding (FSW), was studied. Both the base material (BM) and welded stir zone (SZ) were irradiated with 5 MeV Fe^{++} ions at 450 °C up to 25 displacements per atom (dpa). Characterization was performed using scanning transmission electron microscopy (STEM) and atom probe tomography (APT), with particular emphasis on the Y–Al–O dispersoid characteristics and dislocation microstructures. After irradiation, the dispersoids in the BM increased in diameter and decreased in number density, which was explained by an Ostwald ripening mechanism. FSW caused significant coarsening and agglomeration of the dispersoids. After irradiation, both the diameter and number density of the SZ dispersoids increased, which was explained by an irradiation-enhanced diffusion mechanism. Dislocation loop and network behavior was also characterized and large dislocation loops of ≈20 nm diameter formed by 1 dpa in both the BM and SZ samples, whereas the network density remained nearly constant with irradiation.

Published by Elsevier B.V.

1. Introduction

Small modular reactors (SMRs) have gained popularity as a reactor concept due to smaller capital costs, improved public perception, as well as potential for deployment for humanitarian purposes to disaster-affected zones or to remote destinations where a traditional light water reactor (LWR) would not be feasible. Nevertheless, the total end-of-life dose to core internal components in SMRs can be significant, ranging from 60 to 150 displacements per atom (dpa) and, in the case of next generation (Gen IV) fast reactors, as high as 200 dpa. [1,2]. Microstructural characterization of the irradiated materials is essential for ensuring safety and reliability, but neutron irradiations are costly, time-consuming, and require hot cells for materials examination. Utilizing ion irradiation as a surrogate mitigates many of the challenges associated with neutron irradiation testing [3,4] and self-ion irradiations are unique in that they can reach dose rates of up to 10^{-3} dpa/s, which allows for accelerated irradiation testing with well-controlled temperature, pressure, and dose in candidate structural materials [5–8].

High chromium oxide dispersion-strengthened (ODS) steels are promising materials for usage in SMR, Gen IV, and LWR applications, but little is known about how the material microstructures, particularly those in welded materials, behave under irradiation. Traditional fusion welding processes are unsuitable for joining

* Corresponding author. 590 Holloway Rd, Annapolis, MD, 21042, USA.
E-mail address: getto@usna.edu.edu (E. Getto).

https://doi.org/10.1016/j.jnucmat.2018.12.040
0022-3115/Published by Elsevier B.V.

these alloys because the oxide particles melt or agglomerate during the welding process [9]. Friction stir welding (FSW) is a promising solid-state joining process thought to prevent or mitigate deleterious effects of melting and solidification associated with fusion welding [10–13], but we nevertheless present experimental evidence of yttrium oxide particle agglomeration, coarsening, and phase transformation after FSW of a MA956 ODS steel in the stir zone (SZ) of the weld as well as in the thermo-mechanical heat-affected zone (TMAZ) relative to the base material (BM).

The effect of irradiation on dispersoid stability in MA956 and similar ODS alloys is not well understood. Table 1, adapted from a more extensive review [14], indicates many inconsistencies in the overall literature. The lack of quantitative characterization of dispersoid stability makes conclusive statements difficult, but it appears that dispersoid diameters generally increase with irradiation dose, while the number density tends to stabilize or even decrease as irradiation dose increases. There is no clear relationship with temperature, dose or dose rate. The most comparable study to the present work is from Chen et al. who irradiated MA956 with 3.5 MeV Fe^{++} up to 60, 120 or 180 peak dpa at 450 °C [15]. The authors reported cavities co-located on dispersoids along with an increased diameter of dispersoids and a small decrease in number density at the highest dose of 180 peak dpa.

While there is a significant amount of research on the effect of irradiation on ODS steels or weldments separately [10,11,15–20], only a few simultaneous ion irradiation/welding studies have been performed. Dual ion irradiation (He^{+} and Fe^{+}) of friction stir spot welded (FSSW) PM2000 by C. L. Chen et al. performed at room temperature presented a recovery in the hardness lost during the welding process [21]. During the welding process, elongated, anisotropic grains transformed to more equiaxed grains causing a net decrease in hardness of about 12–23%. On the other hand, the recovery of hardness was due to irradiation hardening from defect clusters or dislocations formed under room temperature irradiation. A similar study on ODS alloy PM2000 welded to 430 steel found similar results after dual beam irradiations also at room temperature [22]. Both the base and welded material exhibited radiation hardening suggesting that the welding and irradiation are in some ways counteracting processes. In contrast, a 12Cr ODS steel weldment irradiated by Guo et al. with 3 MeV Au ions up to 2.7 dpa at 500 °C presented some increase in hardening in both the base metal (BM) and thermo-mechanically affected zone (TMAZ), but not in the stir zone (SZ) of the weld [23]. Voids were also observed in the BM and heat affected zone (HAZ) after irradiation, suggesting a possible link to irradiation-induced swelling.

The limited results in the literature summarized in Table 1 highlighted several major inconsistencies in dispersoid evolution. Moreover, the irradiation dose, ion type, and temperature of welded materials are not comparable to the expected reactor conditions since many are too low in temperature and dose. Finally, the experimental conditions resulting in describing dispersoid evolution results are dissimilar from experiment to experiment which may explain the inconsistencies in the overall trends. Therefore, the objective of this paper is to determine systematically the effect of welding and irradiation on ODS steel MA956 at reactor relevant conditions of 450 °C up to 25 dpa.

1.1. Experiment

Fine-grained (<1 μm) unrecrystallized MA956 steel plate was acquired from Lawrence Livermore National Laboratory. This heat of MA956 was canned and extruded at 1100 °C and hot rolled in three passes at 1100 °C over 4 h with reheating to 1100 °C for 30 min before and after each rolling pass. A precise composition is given in Table 2. Unlike other heats of MA956, no additional heat treament was applied after hot rolling. A 4 mm plate was machined out of the resulting heat treated material.

1.2. Friction stir welding

MegaStir Technologies performed the friction stir welding process [10,24]. The plunge force was maintained constant at 17.8 kN. The tool was fabricated from an MS 80 grade of polycrystalline boron nitride (PCBN) and a convex scroll shoulder step spiral that did not require tilt. The tool had a 25.4 mm diameter shoulder, 1.72 mm pin length and 6 mm pin diameter. No tool contamination was observed. Due to the difficulty of this weld process, a single bead-on-plate run was made on plates of MA956, rather than attempting to join two different base materials. The tool was rotated at 500 revolutions per minute (rpm) and the tool traverse

Table 1
Summary of previous studies of oxide nanoparticle evolution of high Cr (>16Cr) ODS steels from the available literature (n.s. = not stated) adapted and updated from Ref. [14] with permission.

Material	Irrad. Particle	Irrad. Temp. (°C)	Irrad. Dose (dpa)	Dose Rate (dpa/s)	Method	Structure	Chemistry	Size	Number Density	Ref
MA956	3.5 MeV Fe^{++}	450	60–180	n.s.	TEM, HRTEM	monoclinic	$Y_4Al_2O_9$	Increase	Decrease	[15]
MA956	122 MeV Ne^{7+}	440, 570	1–10	n.s.	TEM	Tetragonal (YAT)	n.s.	n.s.	Decrease	[51]
K6	n.s. ion	300–700	20	9.9×10^{-5}	HRTEM	n.s.	n.s.	Stable	Stable	[52]
K1, K4	Fe^{3+}	500–700	20, 150	1×10^{-3}	STEM	n.s.	n.s.	Stable	Stable	[53]
SOC-1	Fe^{3+}	650	60	5×10^{-4}	STEM	n.s.	Stable	Stable	Stable	[54]
18Cr ODS	Fe^{+}	500	4–45	n.s.	EFTEM	Interfaces become irregular	n.s.	Stable	Stable	[55]
18Cr ODS	Fe^{+}	500	150	n.s.	APT, EFTEM	n.s.	Approaches $Y_2Ti_2O_7$ stoichiometry	Increase	Decrease	[18]
18Cr ODS	Au^{2+}	RT	156	n.s.	APT, EFTEM	Amorphization	n.s.	Dissolution	Dissolution	[18]
18Cr ODS	Xe^{+}	27, 500	2.5	n.s.	TEM	Amorphize at $T_{irr} = 27$ °C	n.s.	Increase at $T_{irr} = 27$ °C; else stable	n.s.	[56]
Cr16 ODS, EP450	Bi^{+}, Xe^{+}	350–650	n.s.	n.s.	HRTEM	Amorphous ion tracks	n.s.	Decrease for T_{irr}>600 °C	Stable	[57]
16Cr ODS	e^{-}	500	10	n.s.	TEM	Stable	n.s.	Decrease	Stable	[58]
K3	Fe^{3+}	300, 500	1–10	1×10^{-3}	TEM	n.s.	n.s.	Stable	Stable	[59]
PM2000	Fast n, He^{+}	500	21	n.s.	EFTEM	Amorphization; faceted shape becomes spherical	Cr-rich shells	n.s.	n.s.	[60]

Table 2
Composition of MA956 heat used in this research [11] determined by inductively coupled plasma mass spectrometry and LECO analysis.

Alloy	Fe	Cr	Al	Y_2O_3	Ti	Mn	Si	Ni	C	Mo	S	P
MA956 (wt %)	Bal	19.93	4.75	0.51	0.39	0.09	0.008	0.04	0.023	0.02	0.008	0.006

rate was 25 mm per minute (mmpm). Baker et al. have previously reported on the effects of FSW on the dispersoid size, dispersoid composition, and grain size and in MA956 for a variety of FSW conditions [10–12]. The single welding condition (500 rpm and 25 mmpm) used in the present research causes significant coarsening of the grains, from an equiaxed grain size of 0.89 μm in the BM to 12.5 μm in the SZ [11] and was chosen since it the most severe welding condition that produces fully consolidated welds relative to other heat inputs not published here [10,11].

1.3. Ion irradiation experiments

Electron discharge machining (EDM) was used to excise $10 \times 2 \times 2$ mm rectangular specimens suitable for irradiation from both the BM and the central SZ. The TMAZ region was not analyzed. Prior to irradiation, samples were mechanically ground with SiC paper up to P4000/1200 grit (~5 μm) followed by mechanical polishing to 1 μm diamond polish and a final polish using a vibratory polisher with a 0.05 μm silica solution. Irradiations were performed at Sandia National Laboratories with a 6 MV High Voltage Engineering (HVE) Tandem accelerator. 5 MeV Fe^{++} ions were raster-scanned to create dose rates between $0.44–2.3 \times 10^{-4}$ dpa/s [25] as calculated at a depth of 600 nm using the Quick Kinchin-Pease Mode in the Stopping and Range of Ions in Matter (SRIM) software with a displacement energy of 40 eV per results from Ref. [26]. The resulting calculated damage curve and ion distribution are shown in Fig. 1. Samples were irradiated to 1 (2.62×10^{15} ion/cm^2) and 25 dpa (6.56×10^{16} ion/cm^2) at 450 °C, with the temperature maintained and monitored using a LabView-controlled button heater to a 2σ of 5 °C throughout the course of the irradiation. The irradiation stage was kept under vacuum and pressures were kept at 10^{-5} Pa (10^{-7} Torr) throughout the irradiation.

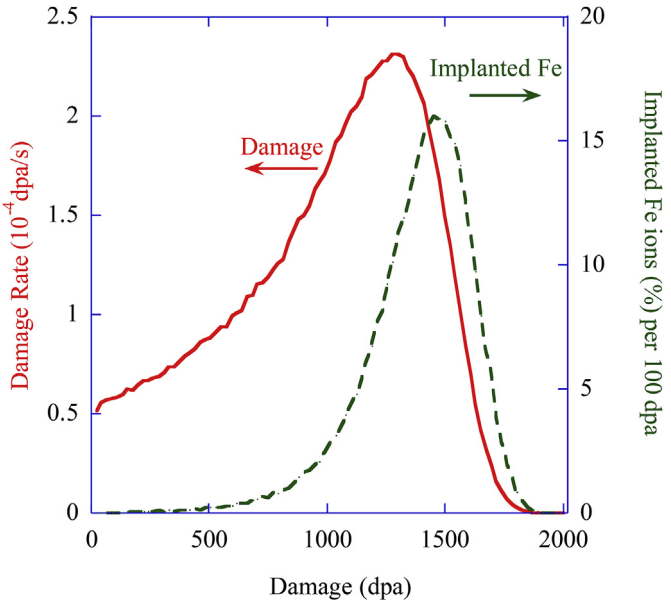

Fig. 1. The damage rate (red solid) is overlaid upon the implanted ion concentration (green dashed) for 5 MeV Fe^{++} in Fe–20Cr. (For interpretation of the references to colour in this figure legend, the reader is referred to the Web version of this article.)

1.4. Microstructural characterization

Because the penetration of 5 MeV Fe^{++} ions is limited to less than 1.6 μm (Fig. 1), transmission electron microscopy (TEM) samples were prepared using a focused ion beam (FIB) liftout method, enabling analysis of the immediate sub-surface microstructure. The plane of the specimens was prepared parallel to the irradiation direction so that the microstructures could be analyzed as a function of depth from the surface. Specimens were thinned to a thickness of no more than 200 nm. One or two liftouts per irradiation condition were analyzed in either a JEOL JEM2200FS or FEI Tecnai TF30-FEG STwin STEM analytic electron microscope (AEM). Images for dispersoid analysis were taken in scanning transmission electron microscope (STEM) mode in bright-field (BF) and STEM high-angle annular dark-field (HAADF) at magnifications of approximately 50,000x. Additional energy dispersive X-ray spectroscopy (EDS) scans were taken to analyze dispersoid composition. The average specimen thickness, needed to estimate dispersoid number density, was measured using the electron energy loss spectroscopy (EELS) zero loss method [27] and was on the order of 150 nm for each sample.

HAADF images were used for quantifying the diameter and number density of the dispersoids. Each dispersoid was counted individually in ImageJ by approximating the dispersoid as a circle and measuring the diameter. The diameter versus depth was calculated by partitioning the depth into 100 nm thick bins, starting from the surface up to 1000 nm. Regions 500–700 nm beneath the surface were selected for detailed analysis since these regions correspond most closely with the calculated doses at 600 nm depth in Fig. 1. The procedure for error analysis was the same as described in detail by Getto et al. for irradiation induced voids due to the similarity between voids and dispersoids in imaging conditions [5].

Dislocation loops and network were imaged using STEM BF in regions 500–700 nm beneath the irradiated surface using the technique described by Parish et al. [28]. Atom probe tomography (APT) tips were prepared from similar regions using the standard liftout technique in a focused ion beam (FIB) using an FEI Nova 600 NanoLab DualBeam SEM/FIB at the Naval Research Laboratory (NRL). APT tips were analyzed in a Cameca LEAP 4000X Si using a 40 K base temperature, 60 pJ nominal laser pulse energy, pulse repetition rate of 200 kHz and a detection rate of 1.5%. Post-analysis data characterization was performed with Cameca's IVAS software where dispersoids were isolated and studied quantitatively using the proximity histogram (or proxigram) technique [29,30].

2. Results

Fig. 2 shows HAADF and BF STEM images of the BM before and after self-ion irradiation. In the HAADF images, Fig. 2a–c, Al–O, Y–Al–O or Y–O precipitates appear darker than the surrounding matrix because STEM HAADF utilizes Z contrast where low atomic species produce less intensity in the image. A protective Pt cap on the surface of each specimen, remnant from the FIB sample preparation, is visible at the top of each micrograph while an oxide (black) formed at the surface under irradiation. The BM microstructure contained a bimodal distribution of ≈10 nm diameter dispersoids throughout the material (Fig. 2a) with some isolated larger precipitates, consistent with previous work [12]. After

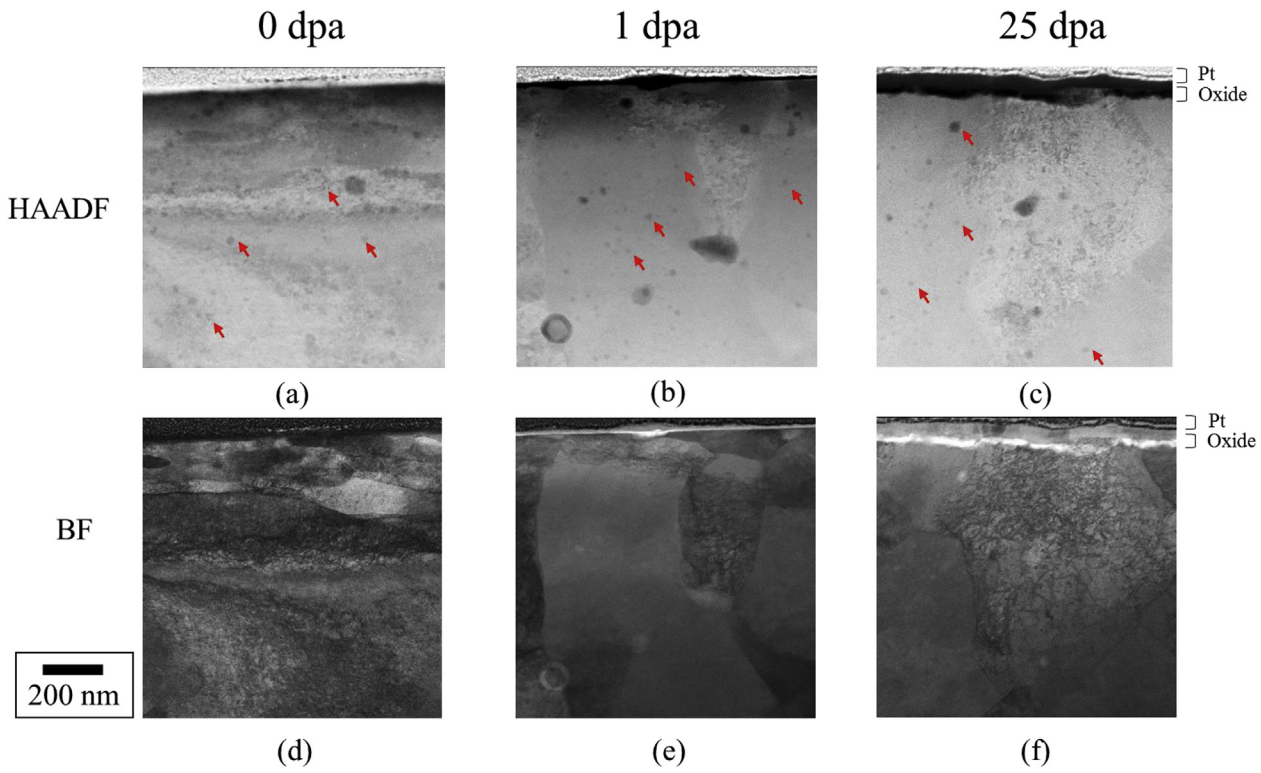

Fig. 2. Corresponding high-angle annular dark-field (HAADF) and bright field (BF) images of the base material of MA956 irradiated with 5 MeV Fe^{++} at 450 °C to a)/d) 0 dpa b)/e) 1 dpa and c)/f) 25 dpa. Red arrows point to small dispersoids. (For interpretation of the references to colour in this figure legend, the reader is referred to the Web version of this article.)

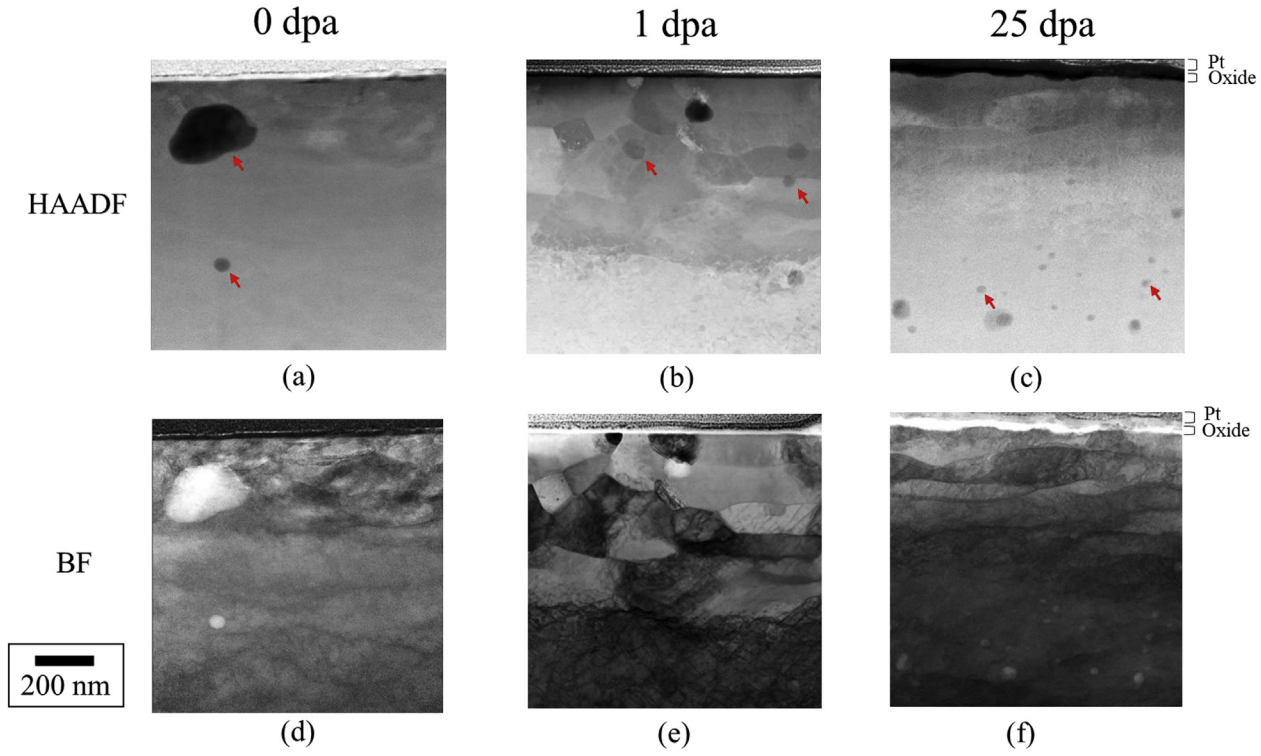

Fig. 3. Corresponding HAADF and BF images of the stir zone of MA956 irradiated with 5 MeV Fe^{++} at 450 °C to a)/d) 0 dpa b)/e) 1 dpa and c)/f) 25 dpa. Red arrows point to small dispersoids. (For interpretation of the references to colour in this figure legend, the reader is referred to the Web version of this article.)

irradiation there is no obvious change in the BM microstructure (Fig. 2b–c), but a quantitative analysis is required to verify this finding. Fig. 2d–f shows STEM BF images of the BM, indicating the high dislocation density before and after irradiation. Here, Y–Al–O dispersoids may appear light or dark depending on orientation, but are difficult to see through the increased diffraction contrast so STEM BF was used strictly for dislocation analysis.

Fig. 3 displays a similar series of STEM images for the SZ. After FSW, Fig. 3a, the dispersoids in the SZ either dissolved into the matrix or agglomerated into larger precipitates, leading to a higher average diameter and lower number density. This alloy's coarsening behavior has been reported previously using scanning electron microscopy (SEM) and APT [12]. After irradiation at 1 dpa, Fig. 3b, smaller dispersoids appeared throughout the microstructure and by 25 dpa, Fig. 3c, even more obvious additional dispersoids formed. Similar to the BF images for the BM, Fig. 3d–f shows a complex microstructure with a high dislocation density in the SZ.

The dispersoids' diameter and number density were quantified from the HAADF STEM images as function of depth as described in the "experimental" section and are compared for the BM and SZ in Fig. 4. From Fig. 4a–c, the diameter of dispersoids is consistently smaller in the BM relative to the SZ throughout the depth and across all doses examined. Fig. 4d–f presents the number density of dispersoids from 0 to 1000 nm. At 0 dpa (Fig. 4d), the low number density is consistent with the coarsening behavior from welding observed in previous studies [12] that was attributed to an Ostwald ripening process. The number density of the SZ dispersoids increases after irradiation, as demonstrated in Fig. 4e and f.

Due to the peaked irradiation profile, shown in Fig. 1, it is more appropriate to consider the microstructures present 500–700 nm beneath the surface to limit dose variation from the reported dose at 600 nm. Fig. 5 presents the distribution of dispersoids in the 500–700 nm region of interest. The dispersoid size distribution in the BM (Fig. 5a) exhibits a sharp peak near 8 nm diameter with a few larger dispersoids. After welding, Fig. 5d, the dispersoid size distribution is much flatter; however, there were only 24 precipitates counted limiting the statistical analysis compared to the base case. After irradiation, the distribution tended to flatten out for the BM (Fig. 5b and c) indicating that there was some growth of the overall size of the dispersoids. Dispersoid growth behavior was also observed in the SZ after irradiation, Fig. 5e and f, but there also appeared to be more, smaller precipitates at 1 and 25 dpa relative to 0 dpa. This suggests there may be re-precipitation of dispersoids that were dissolved during the welding process.

To investigate this hypothesis, the microstructures in the BM and SZ after irradiation at 25 dpa were examined by APT, as shown in Fig. 6. The irradiated BM contains a high number density of small (≈2–10 nm diameter) Y–Al–O dispersoids with a Y:Al ratio near unity, and are thus identified as $YAlO_3$ (yttrium aluminum perovskite, YAP). This is consistent with the BM dispersoids studied previously by APT for the unirradiated BM material [12]. Irradiation-induced dislocations and sub-grain boundaries, to

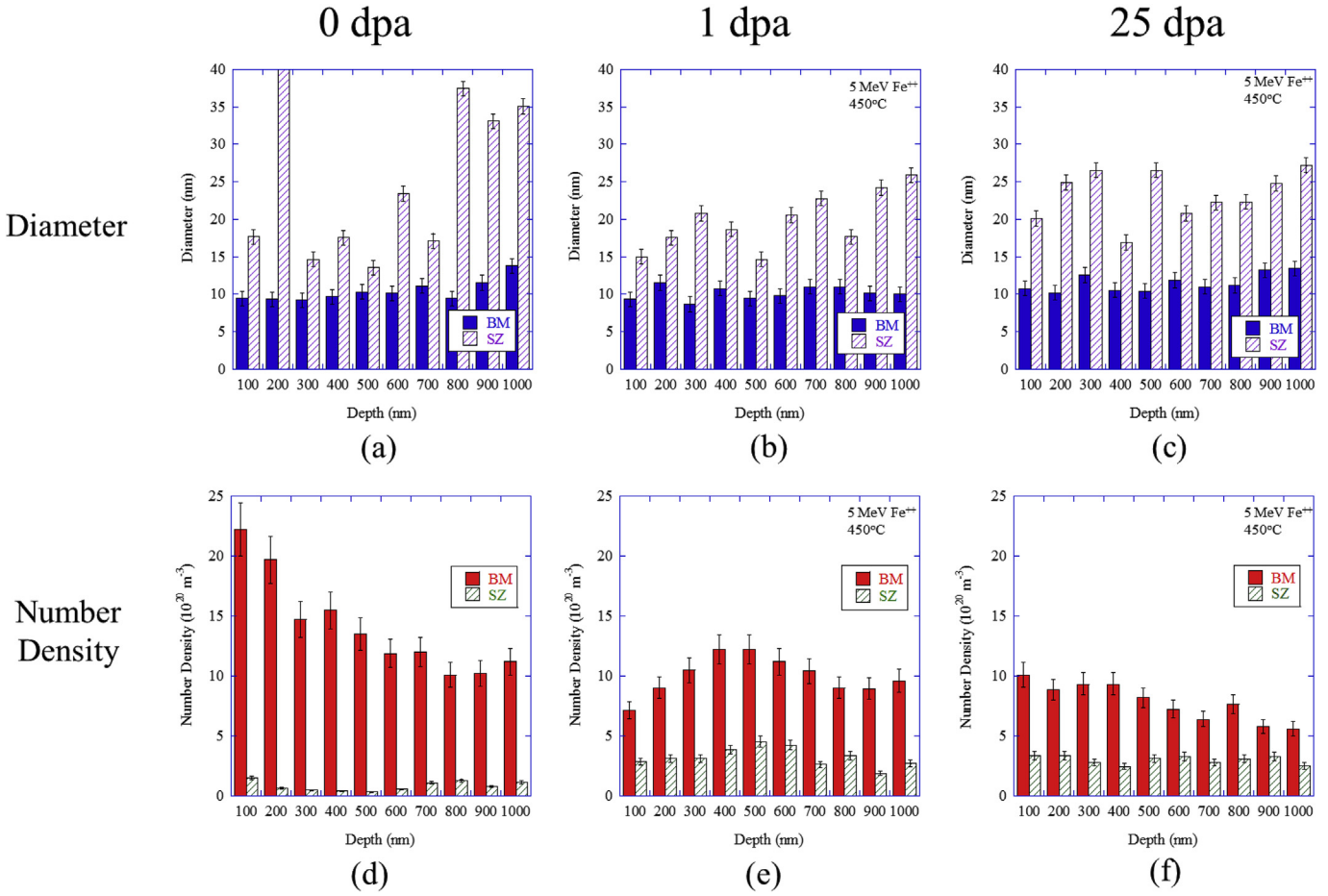

Fig. 4. Comparison of dispersoid depth distribution in terms of diameter for base material (solid blue) and stir zone (striped purple) at a) 0[1] b) 1 and c) 25 dpa. Comparison of dispersoid depth distribution in terms of number density of base material (solid red) and stir zone (striped green) at d) 0 e) 1 and f) 25 dpa. (For interpretation of the references to colour in this figure legend, the reader is referred to the Web version of this article.)

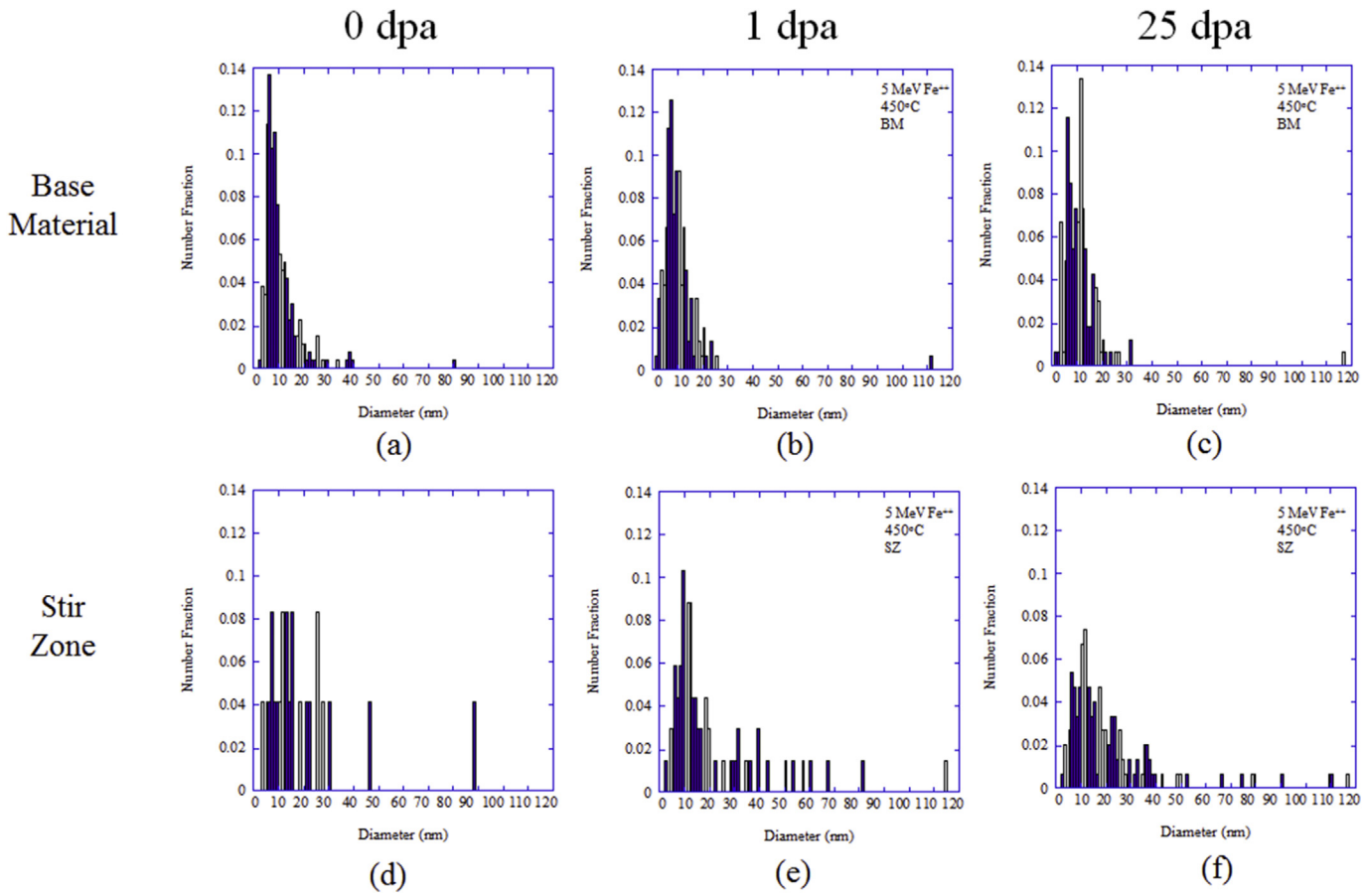

Fig. 5. Distribution of dispersoids in the 500–700 nm depth region observed in MA956 irradiated with 5 MeV Fe^{++} up to 25 dpa at 450 °C. a)-c) show distributions of dispersoids in the base material at 0, 1 and 25 dpa, respectively, whereas d)-f) show distributions in the stir zone at 0, 1, and 25 dpa, respectively.

which Ti and C segregate (Fig. 6b), are also apparent. Associated with these dislocations/sub-grains are larger, O-rich particles. These may have formed heterogeneously on the dislocations during elevated-temperature irradiation, or may have been present prior to irradiation and, because of their larger size, may have acted as sites onto which the dislocations piled on. These larger particles are distinct from the more numerous YAP dispersoids in that they contain mostly Al and O with very little Y.

APT analysis of the irradiated SZ microstructure failed to intercept any of the large agglomerated and coarsened Y–Al–O oxides, which is a result of their small number density (Fig. 4). Analysis of the irradiated SZ material did, however, reveal the presence of small (≈5–7 nm diameter) Y–Al–O dispersoids, which were not observed in previous APT analysis of similar friction stir welds prior to irradiation [12]. Comparing the proxigrams in Fig. 6, these dispersoids appear to be similar in size and composition to those in the BM and are believed to be $YAlO_3$ (yttrium aluminum perovskite, YAP) that precipitated during irradiation at 450 °C. The SZ also contains irradiation-induced dislocations, Fig. 6e, and these precipitated dispersoids are often associated with these defects.

The dislocation structure in the irradiated materials was also examined by STEM and representative STEM BF images are shown in Fig. 7. Prismatic dislocation loops are pervasive throughout the material. The complexity of the microstructures makes loop identification difficult, but identified loops were **a**<100> or **a/2**<111>, consistent with other ferritic alloys [31]. A summary of quantitative microstructure results is presented in Table 3.

3. Discussion

3.1. Dispersoid evolution

This particular heat of MA956 has been analyzed and reported on using SEM and APT, but not previously by TEM/STEM. Therefore, the STEM characterization at 0 dpa for welded and base material is presented first as a benchmark for the irradiated cases.

3.1.1. Comparison of dispersoid behavior between base material and stir zone

Fig. 8 presents a quantification of the diameter and number density data from Fig. 4 confined to the 500–700 nm depth region so as to be consistent with irradiated specimens. APT results from a previously study on the MA956 BM showed an average diameter of 7.2 nm versus 10.6 nm in this study [12] indicating that APT and STEM are resulting in comparable quantitative results. With welding, coarsening of the dispersoids was clearly observed. The average diameter increased from 10.6 to 19.2 nm and the number density decreased from 8.96 to 0.593×10^{20} m^{-3}. Similar behavior was observed in Ref. [11] and attributed to an Ostwald ripening process. Baker et al. observed coarsening of the dispersoids from the BM to the SZ in APT and SEM from 7.2 nm to 410 nm, respectively. It is reasonable to expect the average dispersoid size would be smaller in TEM, as the resolution is much higher (~1–2 nm versus ~10–20 nm in TEM and SEM, respectively) and the samples are much thinner (~150 nm). Coarsening of the dispersoids during the weld process has been observed extensively in other heats of

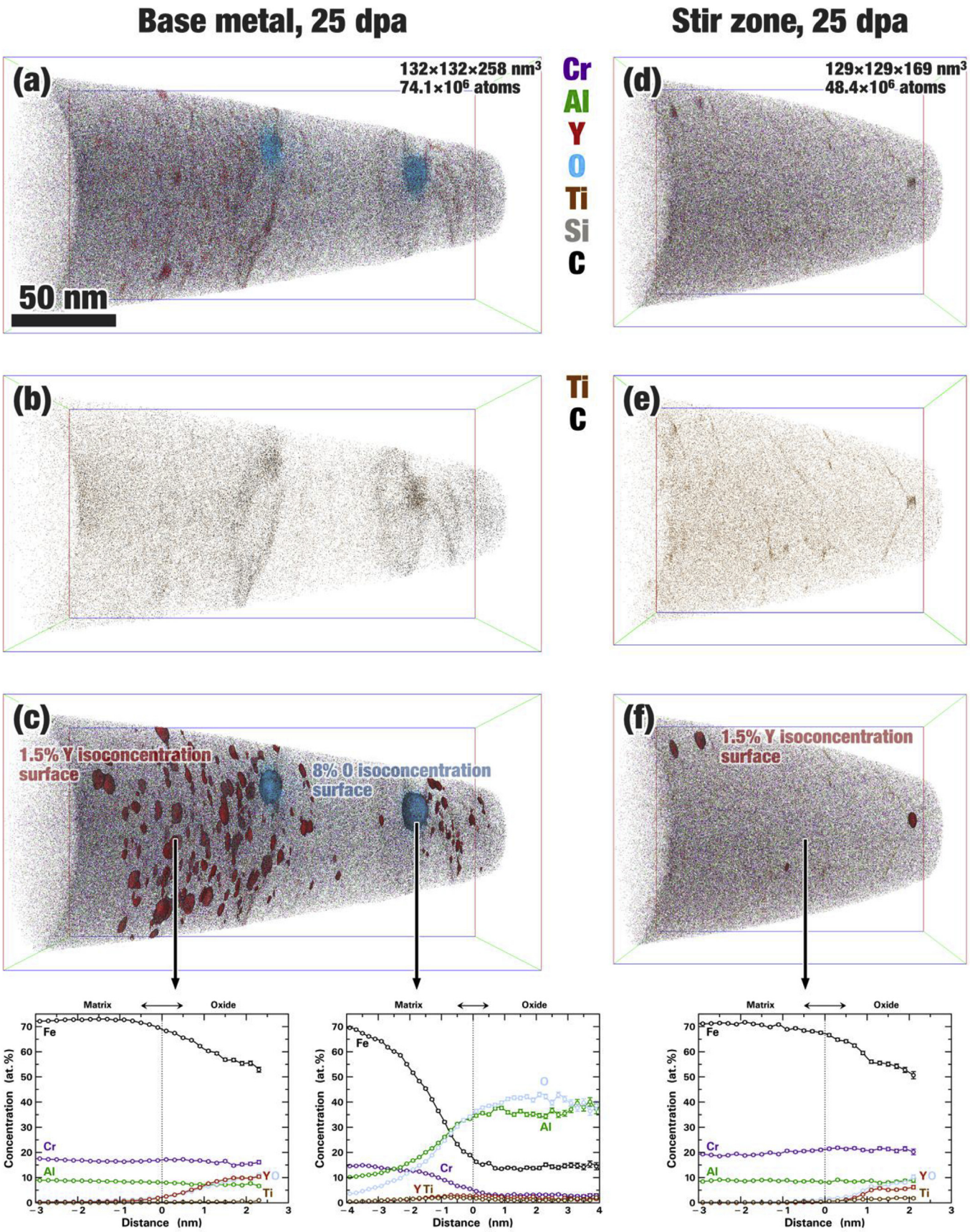

Fig. 6. APT reconstructions of the BM and SZ after 25 dpa irradiation.

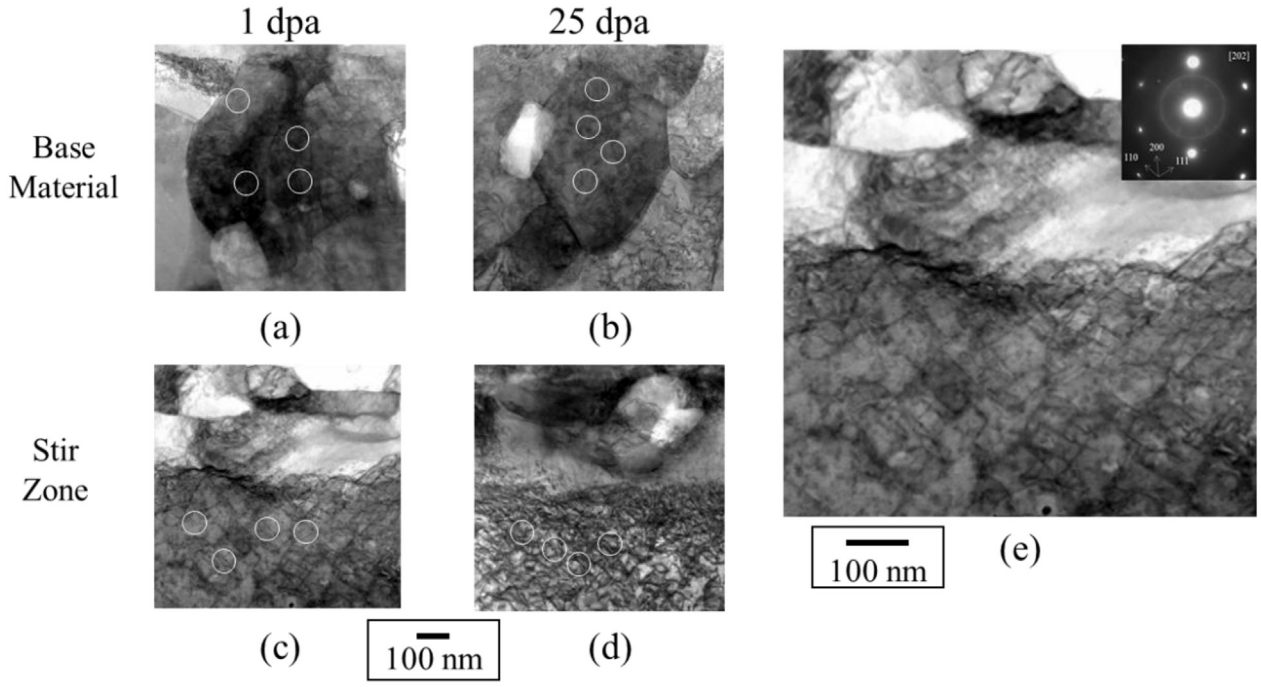

Fig. 7. STEM BF images of dislocation loops and network in base material at a) 1 and b) 25 dpa and stir zone of MA956 at c) 1 and d) 25 dpa. Diffraction pattern used in analyzing the 1 dpa stir zone as an example is included in e). White circles identify selected loops.

Table 3
Summary of microstructure characterization results in MA956 irradiated with 5 MeV Fe^{++} in the depth region of 500–700 nm. All results were from STEM imaging.

		Y–Al–O Dispersoids			Dislocation			
Dose (dpa)	Sample Type	Number of Precipitates	Precipitate diameter (nm)	Precipitate Density (10^{20} m^{-3})	Number of Loops	Loop Diameter (nm)	Dislocation Loop Density (10^{20} m^{-3})	Dislocation line density (10^{14} m^{-2})
0	BM	263	10.6 ± 1.0	8.96 ± 0.90	NA	NA	NA	0.614 ± 0.061
0	SZ	24	19.2 ± 1.0	0.593 ± 0.059	NA	NA	NA	0.532 ± 0.053
1	BM	393	10.4 ± 1.0	10.8 ± 1.1	17	20.2 ± 1.0	6.18 ± 0.62	1.17 ± 0.12
1	SZ	68	21.4 ± 1.0	3.43 ± 0.34	32	19.7 ± 1.0	5.78 ± 0.58	1.38 ± 0.14
25	BM	164	11.5 ± 1.0	5.13 ± 0.51	40	20.6 ± 1.0	6.27 ± 0.63	0.716 ± 0.072
25	SZ	149	21.4 ± 1.0	2.06 ± 0.21	35	15.6 ± 1.0	10.3 ± 1.0	0.595 ± 0.060

MA956 and other ODS alloys [32,33]. For instance, West et al. welded together two plates of MA956 with a W–Re tool with a rotation speed was 600 rpm with a travel speed of 13 mm/min and the welded material experienced similar coarsening of the dispersoids [32].

3.1.2. Effect of irradiation on dispersoid evolution in the base material

As a benchmark, and to be consistent with previous results from the literature, the evolution of the dispersoids with irradiation in the BM is examined first. The average diameter and number density from the 500–700 nm region is plotted in Fig. 9a. Diameter was similar between 0 and 1 dpa (10.6 versus 10.4 nm), but increased to 11.5 nm by 25 dpa. Although the average diameter increase was small, the dispersoid distribution in Fig. 5 has shifted to the right indicating some small amount of growth. The decrease in number density from 8.96 to 5.13 × 10^{20} m^{-3} was more statistically significant. This may be evidence of some small amount of coarsening that would likely continue up to higher doses. When compared with results from the literature summarized in Table 1, Fig. 9a mostly matches the behavior reported by Chen et al. and [15] and Lescoat et al. [18], though calling the dispersoids stable is certainly debatable especially when considering the qualitative similarity noted earlier in Fig. 2a–c.

A survey of the current literature from Wharry et al. [14] proposed multiple mechanisms for the coarsening of dispersoids or nanoprecipitates under irradiation. First, an Ostwald ripening mechanism proposes that smaller dispersoids dissolve and are redeposited on larger, more stable precipitates. This has been used to explain effect of welding and irradiation and therefore is attractive as a mechanism [34,35]. Irradiation-enhanced diffusion has also been used to explain clustering and formation of new dispersoids of a smaller size or growth of existing dispersoids by solute diffusion to the stable dispersoids or nucleation at new sites [18,36]. In this case, it is expected that increased diameter and number density would be observed. Other mechanisms that have been proposed include ballistic dissolution [36,37], which may cause a decrease in diameter and number density. Finally, there may be multiple active mechanisms depending on the pre-existing microstructure. If different mechanisms are dominant depending on the initial processing and microstructure of the alloys, this may help to explain the disparate behaviors noted in Table 1.

3.1.3. Effect of irradiation on dispersoid evolution in the stir zone

The behavior of dispersoids under systematic irradiation after the FSW welding process, Fig. 9b, represents first of its kind data at

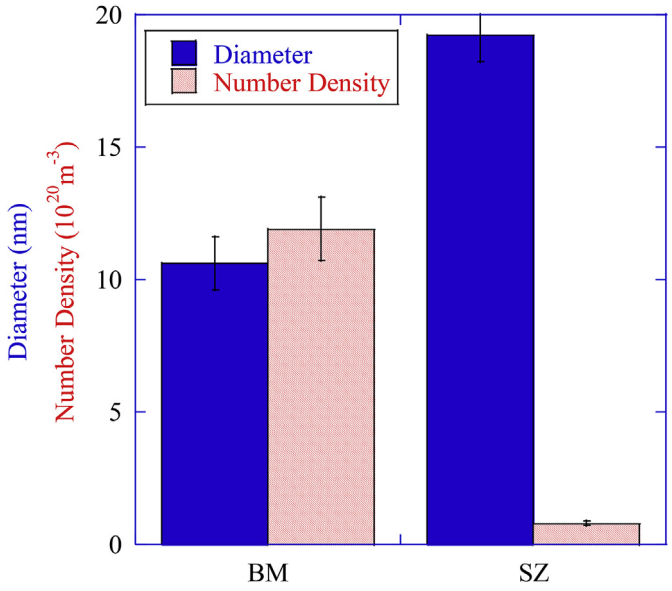

Fig. 8. Comparison of dispersoid diameter (solid blue) and number density (red striped) for base material and stir zone of MA956 prior to irradiation. (For interpretation of the references to colour in this figure legend, the reader is referred to the Web version of this article.)

relevant LWR operating temperatures. In contrast to Fig. 9a for the BM, Fig. 9b demonstrates both the diameter and number density of the dispersoids in the SZ increased with irradiation up to 25 dpa. Average diameter increased from 19.2 nm to 21.4 nm whereas average number density increased from 0.593 to 2.06 × 10^{20} m^{-3}. Two simultaneous processes may explain this behavior. First, coarsening of the existing dispersoids may be increasing the diameter similar to behavior observed in the base material in Fig. 9a. At the same time, smaller precipitates were observed in Fig. 2e and f and Fig. 6d–f, that did not appear in the welded, unirradiated case (Fig. 2d). Thus, the increasing number density may be explained by re-precipitation of solute that was forced into solution during the heat and mechanical action associated with FSW. This type of behavior is best explained by the irradiation-enhanced diffusion mechanism [18,36]. For example, the non-equilibrium welding process creates a microstructure susceptible to re-precipitation of the Y–Al–O or Y–O that was in the welded matrix. Irradiation provides the driving force toward re-precipitation, as well as solute diffusion toward the stable surviving dispersoids causing increases in both average diameter and number density of the dispersoids. Moreover, irradiation provides additional dislocations that may serve as nucleation sites.

After welding, the volume fraction of dispersoids decreased from 0.23% to 0.12%, suggesting that some of the preexisting dispersoids dissolved. During the FSW process, the temperature inside of the weld has been estimated to be approximately 90% of the melting temperature [16,38]. Due to this high heat input, dissolution of the precipitates is reasonable and has been suggested as a primary mechanisms for changes in the dispersoid microstructure [32] in addition to Ostwald coarsening or agglomeration [10,12]. Although the formation energies for Y–Al–O are quite high, ~1827 kJ/mol up to 7197 kJ/mol [10], small precipitates are much less stable and closer to the critical radius so the high heat input may drive the precipitates back into solution. Furthermore, it is reasonable to suggest that irradiation/radiation-enhanced diffusion can provide the driving force to re-precipitate Y–Al–O back into solution.

To verify that the phases forming are dispersoids as opposed to irradiation-induced voids or another phase, EDS was performed. Fig. 10 shows an EDS scan with a suspected dispersoid in the lower left corner of the image. There is an outline of Y, Al and O (with the Y–O signal the strongest) where the dispersoid is expected from the HAADF image. The Al concentration in MA956 is 4.75 wt% whereas Ti concentration is 0.39 wt%, which is why these dispersoids tend to be Y–Al–O rather than Y–Ti–O. The formation of Y–Al–O dispersoids is different in MA956 than many other ODS alloys with lower Al concentration where Y–Ti–O dispersoids tend to form predominantly [39]. There was a clear correlation of

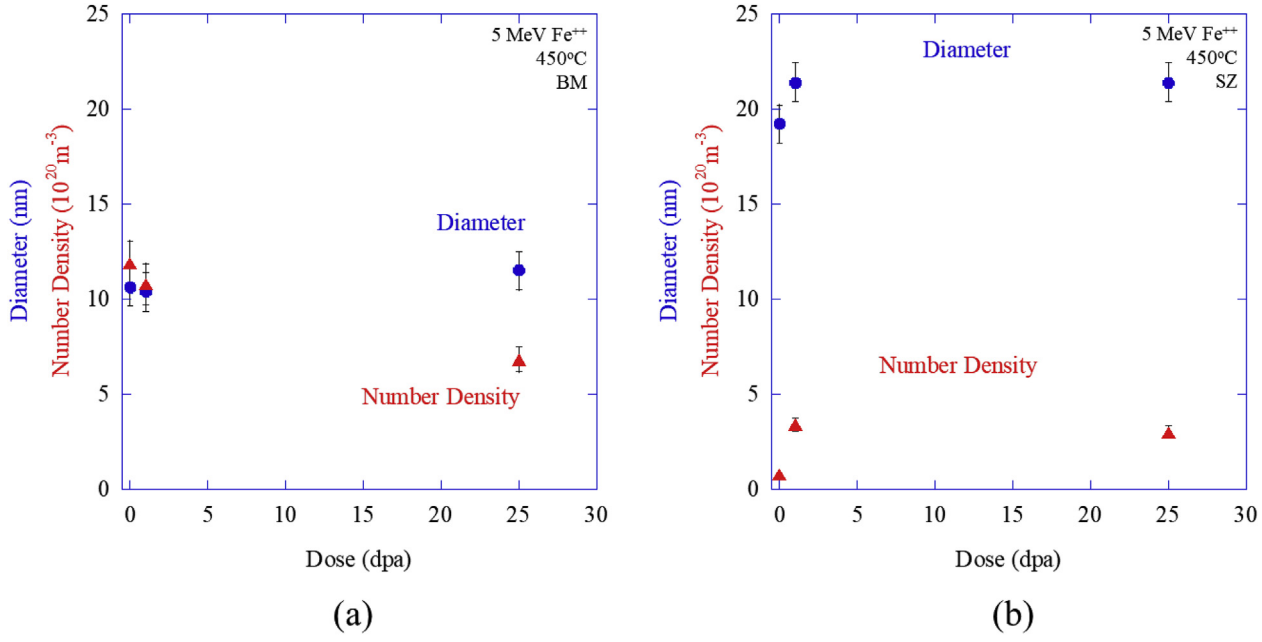

Fig. 9. Evolution of dispersoid diameter (blue circles) and number density (red triangles) in a) base material and b) stir zone of MA956 irradiated with 5 MeV Fe^{++} up to 25 dpa at 450 °C. (For interpretation of the references to colour in this figure legend, the reader is referred to the Web version of this article.)

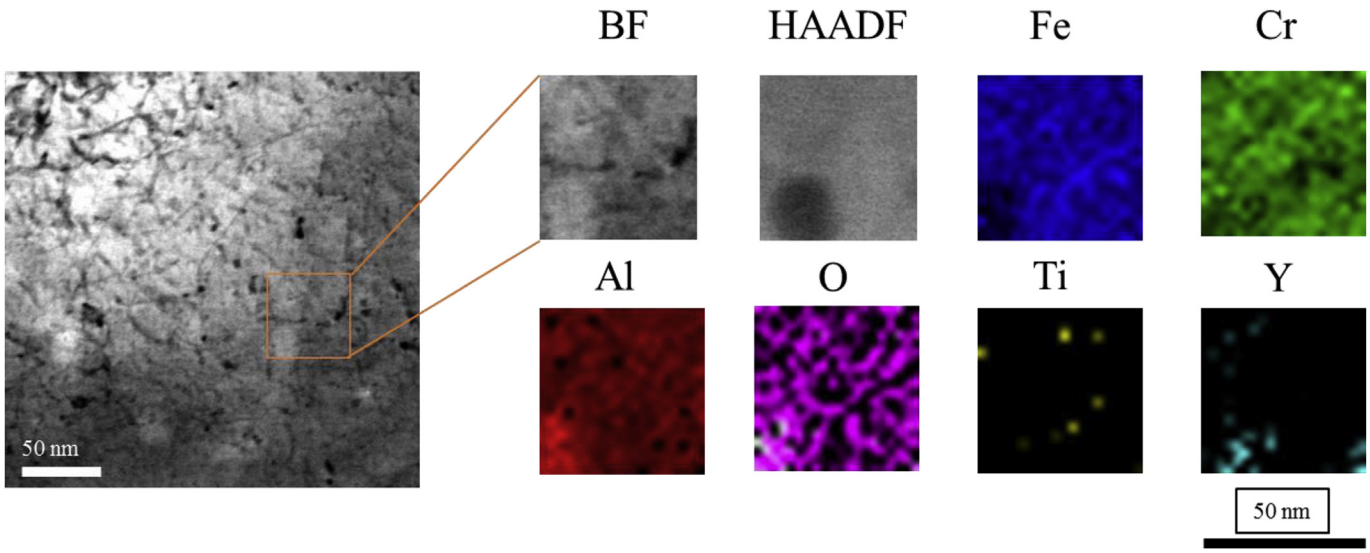

Fig. 10. STEM BF image with EDS scan showing distribution of Fe, Cr, Al, O, Ti and Y in base material of MA956 irradiated with 5 MeV Fe^{++} at 450 °C to 25 dpa.

Y–Al–O with the black dot features that have been identified as dispersoids in other scans that were not presented here.

3.1.4. Comparison of dispersoid behavior at 25 dpa

Finally, the irradiated dispersoids are directly compared in Fig. 9. Relative to the same comparison at 0 dpa, the welded diameter is still approximately ~9–10 nm larger. In contrast, the number density is much closer between the SZ and BM case ($8.96–0.593 \times 10^{20}$ m^{-3} at 0 dpa versus 5.13 to 2.06×10^{20} m^{-3} at 25 dpa). This has potentially interesting implications for the mechanical properties. Softening due to the welding process has been observed in MA956 and similar alloys [10,21,32], and re-precipitation of dispersoids with irradiation may recover some of the lost strength also observed by Chen et al. and Guo et al. [22,23].

Starting microstructure has been shown to be key in understanding the variation in radiation tolerance of many alloys [7,23,40]. In this case, it is key in understanding the evolution of dispersoids with either welding or irradiation. Potentially, the BM and welded microstructure are becoming more similar as irradiation reverses some of the effect of welding by re-precipitation of dissolved dispersoids. In fact, an argument could be made that the microstructures are converging towards each other, though high doses are necessary to determine if that trend will continue. A possible explanation may be that the highly disparate starting conditions of the same alloy, induced by welding, influence the overall trends in dispersoid evolution. Thus, the behavior of the BM is better explained by Ostwald ripening whereas the welding is more consistent with the irradiation-enhanced diffusion mechanism. Higher dose irradiations and irradiations at other temperatures may clarify and confirm this.

For now, these results are a promising as a first approach to assessing the viability of not only ODS but more importantly, advanced joining techniques, both of which are necessary to implementation of new and advanced reactor concepts. Furthermore, the relative stability of the base material reported herein is very promising and we conclude that MA956 should be considered as a viable option along with other ODS alloys currently under consideration by reactor designers.

3.2. Dislocation behavior

The evolution of dislocation loops are shown in the BM in Fig. 7a,c and SZ in Fig. 7b,d. Fig. 7e includes the diffraction pattern for the analyzed grain (450 °C, SZ) such that **a**<100> and ½**a**<111>. The loops were compared in either direction and 88% of loops were **a**<100>. This is consistent with previous results from neutron [31,41] and ions [5,42] of MA956 and other high chromium (>10 wt % Cr) alloys. Regardless of welding condition, large dislocation loops (~20 nm) formed by 1 dpa and remained fairly constant up to 25 dpa, shown in Fig. 11. There was some decrease in loop diameter in the stir zone from 1 to 25 dpa. Number density was constant for the base material and increased by a factor of 2 for the welded sample. Dislocation loop size tends to be primarily controlled by irradiation temperature [43], whereas dislocation number density tends to saturate by ~10 dpa [44–48] though some evolution at higher doses in ferritic martensitic alloys has been reported [40,41]. However, number density measurements can be quite variable (as much as a factor of two) depending on the local sample thicknesses or imaging conditions. It is clear that a greater number of smaller dislocation loops formed in the welded region under irradiation. Radiation induced segregation of Ti to the dislocations was observed in the weld at 25 dpa in Fig. 6b,e.

Network dislocations were imaged via the method described by Xu in Ref. [49]. A STEM image of the network dislocations tangled on a dispersoid is shown in Fig. 12a, which was quite similar to that shown by atom probe in Fig. 6e. The unirradiated base material and stir zone had starting network dislocation densities of 6.14 and 5.32×10^{13} m^{-2}, respectively, which was nearly within error bars. Fig. 12b shows that with irradiation, there was a small increase in density. The stability of the network is consistent with previous results that show network density is fairly stable even up to high doses [40] in ferritic-martensitic alloys.

4. Conclusions

A first approach to address the viability of friction stir welding of MA956 as a processing technique of this candidate reactor structural material was assessed experimentally by the combination of friction stir welding and ion irradiation with post irradiation microstructure characterization and the following was concluded.

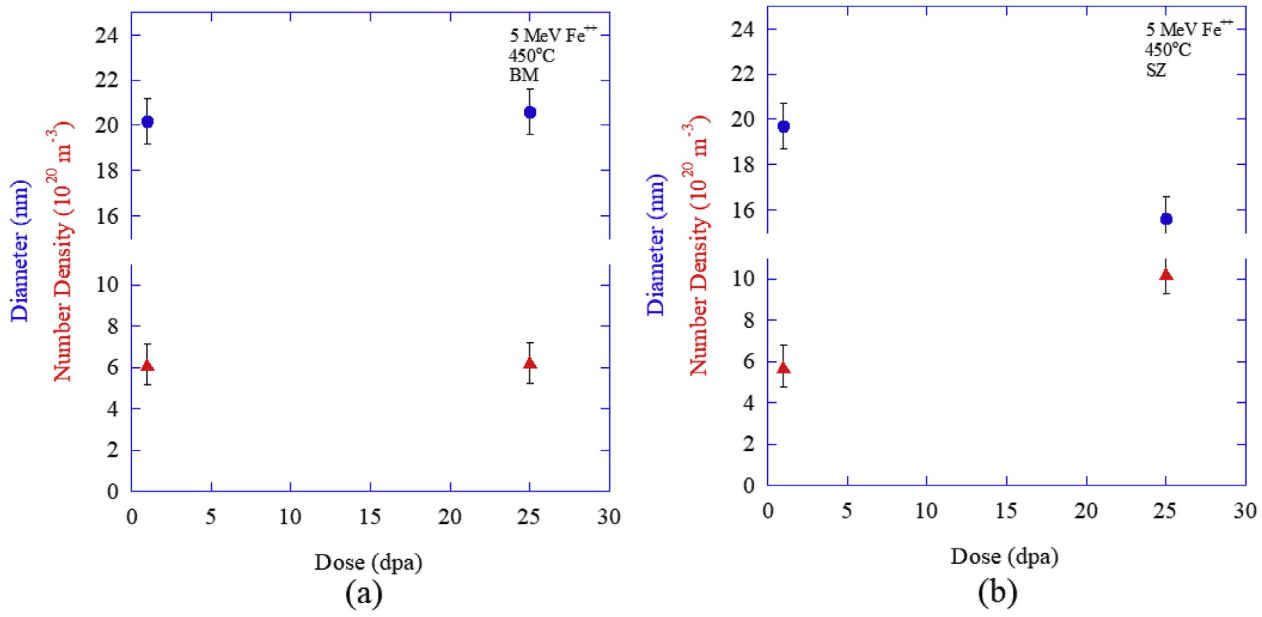

Fig. 11. Evolution of dislocation loop diameter (blue circles) and number density (red triangles) in a) base material and b) stir zone of MA956 irradiated at 450 °C up to 25 dpa. (For interpretation of the references to colour in this figure legend, the reader is referred to the Web version of this article.)

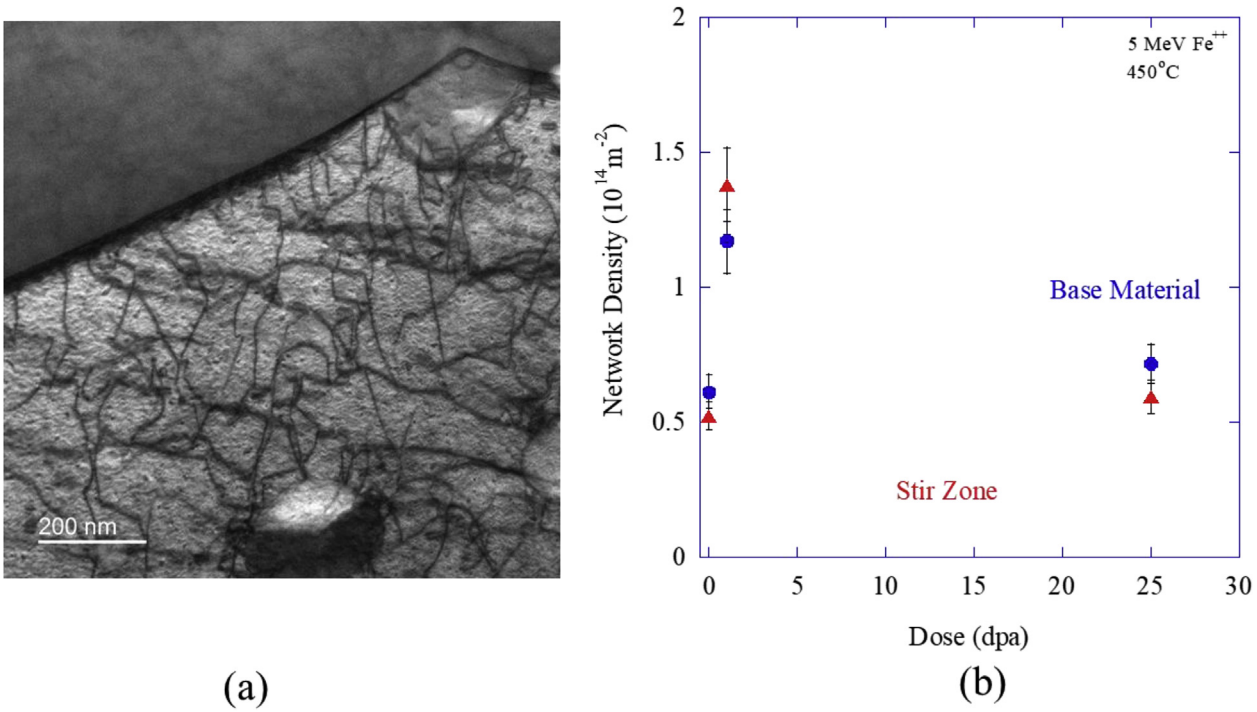

Fig. 12. a) STEM BF image of network dislocation tangles in unirradiated stir zone of MA956. b) Network dislocation density in MA956 irradiated with 5 MeV Fe^{++} at 450 °C up to 25 dpa. Base material is shown by blue circles and stir zone by red triangles. (For interpretation of the references to colour in this figure legend, the reader is referred to the Web version of this article.)

- The dispersoids in the base material of MA956 increased in diameter and decreased in number density with 5 MeV Fe^{++} up to 25 dpa at 450 °C, which can be explained by an Ostwald Ripening mechanism.
- After friction stir welding, there was coarsening of the dispersoids relative to the base material. After irradiation, both the diameter and number density increased, which was explained by an irradiation-enhanced diffusion mechanism.
- Dislocation loop and network behavior was characterized up to 25 dpa. Large dislocation loops of ~20 nm formed by 1 dpa in both base material and stir zone samples whereas the network density remained more or less constant with irradiation.

Future efforts to increase the library of MA956 sample conditions at higher dose with the reactor operating envelope are already underway so as to provide more evidence for suitability of MA956

in next generation reactors.

Acknowledgements

Research supported by the Defense Threat Reduction Agency (DTRA) and a United States Naval Academy Midshipman Research Support Grant. This work was also supported by the U.S. Department of Energy, Office of Nuclear Energy under DOE Idaho Operations Office Contract DE-AC07- 051D14517 as part of a Nuclear Science User Facilities experiment NSUF RTE 17-906. The work was performed, in part, at the Center for Integrated Nanotechnologies, an Office of Science User Facility operated for the U.S. Department of Energy (DOE) Office of Science. Sandia National Laboratories is a multi-mission laboratory managed and operated by National Technology and Engineering Solutions of Sandia, LLC. a wholly owned subsidiary of Honeywell International, Inc., for the U.S. Department of Energy's National Nuclear Security Administration under contract DE-NA-0003525. This paper describes objective technical results and analysis. Any subjective views or opinions that might be expressed in the paper do not necessarily represent the views of the U.S. Department of Energy or the United States Government. The authors gratefully acknowledge D. Buller for assistance in ion irradiation and T. Brintlinger and Y. Wu for assistance on the TEMs.

Appendix A. Supplementary data

Supplementary data to this article can be found online at https://doi.org/10.1016/j.jnucmat.2018.12.040.

Data availability statement

Data used in this work is permanently available in archive ref [50].

References

[1] S.M. Bruemmer, M.A. Catalan, D. Sandusky, W. Lunceford, Assessment of Materials Issues for Light-water Small Modular Reactors, 2013.
[2] Chapter Four: “Reactor,” in: NuScale Stand. Plant Des, Certif. Appl., 2016.
[3] G.S. Was, Z. Jiao, E. Getto, K. Sun, A.M. Monterrosa, S.A. Maloy, O. Anderoglu, B.H. Sencer, M. Hackett, Emulation of reactor irradiation damage using ion beams, Scripta Mater. 88 (2014) 33–36, https://doi.org/10.1016/j.scriptamat.2014.06.003.
[4] G.S. Was, J.T. Busby, T. Allen, E. Kenik, A. Jenssen, S.M. Bruemmer, J. Gan, A.D. Edwards, P.M. Scott, P. Andresen, Emulation of neutron irradiation effects with protons: validation of principle, J. Nucl. Mater. 300 (2002) 198–216, https://doi.org/10.1016/S0022-3115(01)00751-6.
[5] E. Getto, Z. Jiao, A.M. Monterrosa, K. Sun, G.S. Was, Effect of pre-implanted helium on void swelling evolution in self-ion irradiated HT9, J. Nucl. Mater. (2015), https://doi.org/10.1016/j.jnucmat.2015.01.045.
[6] E. Getto, G. Vancoevering, G.S. Was, The co-evolution of microstructure features in self-ion irradiated HT9 at very high damage levels, J. Nucl. Mater. 484 (2017) 193–208, https://doi.org/10.1016/j.jnucmat.2016.12.006.
[7] X. Wang, Q. Yan, G.S. Was, L. Wang, Void swelling in ferritic-martensitic steels under high dose ion irradiation: exploring possible contributions to swelling resistance, Scripta Mater. (2015) 6–11, https://doi.org/10.1016/j.scriptamat.2015.08.032.
[8] M.B. Toloczko, F. a. Garner, V.N. Voyevodin, V.V. Bryk, O.V. Borodin, V.V. Mel'nychenko, A.S. Kalchenko, Ion-induced swelling of ODS ferritic alloy MA957 tubing to 500 dpa, J. Nucl. Mater. (2014), https://doi.org/10.1016/j.jnucmat.2014.06.011.
[9] M.G. McKimpson, D.O. Donnell, Joining ODS materials for high. Temperature applications, J. Occup. Med. 957 (1994) 956–958.
[10] B.W. Baker, E.S.K. Menon, T.R. McNelley, L.N. Brewer, B. El-Dasher, J.C. Farmer, S.G. Torres, M.W. Mahoney, S. Sanderson, Processing-microstructure relationships in friction stir welding of MA956 oxide dispersion strengthened steel, Metall. Mater. Trans. E. 1 (2014) 318–330, https://doi.org/10.1007/s40553-014-0033-6.
[11] B.W. Baker, T.R. McNelley, L.N. Brewer, Grain size and particle dispersion effects on the tensile behavior of friction stir welded MA956 oxide dispersion strengthened steel from low to elevated temperatures, Mater. Sci. Eng. 589 (2014) 217–227, https://doi.org/10.1016/j.msea.2013.09.092.
[12] B.W. Baker, K.E. Knipling, L.N. Brewer, Oxide particle growth during friction stir welding of fine grain MA956 oxide dispersion strengthened steel, Metall. Mater. Trans. E. (2017) 1–12, https://doi.org/10.1007/s40553-016-0101-1.
[13] B.W. Baker, L.N. Brewer, Joining of oxide dispersion strengthened steels for advanced reactors, JOM (J. Occup. Med.) 66 (2014) 2442–2457, https://doi.org/10.1007/s11837-014-1206-6.
[14] J.P. Wharry, M.J. Swenson, K.H. Yano, A review of the irradiation evolution of dispersed oxide nanoparticles in the b.c.c. Fe-Cr system: current understanding and future directions, J. Nucl. Mater. 486 (2017) 11–20, https://doi.org/10.1016/j.jnucmat.2017.01.009.
[15] T. Chen, H. Kim, J.G. Gigax, D. Chen, C.C. Wei, F.A. Garner, L. Shao, Radiation response of oxide-dispersion-strengthened alloy MA956 after self-ion irradiation, Nucl. Instrum. Methods Phys. Res. Sect. B Beam Interact. Mater. Atoms 409 (2017) 259–263, https://doi.org/10.1016/j.nimb.2017.05.024.
[16] R.S. Mishra, Z.Y. Ma, Friction stir welding and processing, Mater. Sci. Eng. R Rep. 50 (2005) 1–78, https://doi.org/10.1016/j.mser.2005.07.001.
[17] B. Jasthi, S. Howard, W. Arbegast, G. Grant, S. Koduri, D. Herling, Friction Stir Welding of MA 957 Oxide Dispersion Strengthened Ferritic Steel, in: Frict. Stir Weld. Process, vol. III, 2005, pp. 75–79.
[18] M.L. Lescoat, J. Ribis, Y. Chen, E.A. Marquis, E. Bordas, P. Trocellier, Y. Serruys, A. Gentils, O. Kaïtasov, Y. De Carlan, A. Legris, Radiation-induced Ostwald ripening in oxide dispersion strengthened ferritic steels irradiated at high ion dose, Acta Mater. 78 (2014) 328–340, https://doi.org/10.1016/j.actamat.2014.06.060.
[19] C.H. Zhang, Y.T. Yang, Y. Song, J. Chen, L.Q. Zhang, J. Jang, A. Kimura, Irradiation response of ODS ferritic steels to high-energy Ne ions at HIRFL, J. Nucl. Mater. 455 (2014) 61–67, https://doi.org/10.1016/j.jnucmat.2014.04.015.
[20] N. Baluc, D.S. Gelles, S. Jitsukawa, A. Kimura, R.L. Klueh, G.R. Odette, B. van der Schaaf, J. Yu, Status of reduced activation ferritic/martensitic steel development, A, J. Nucl. Mater. (2007) 367–370, https://doi.org/10.1016/j.jnucmat.2007.03.036, 33–41.
[21] C.L. Chen, A. Richter, R. Kögler, L.T. Wu, Dual-beam irradiation of friction stir spot welding of nanostructured ferritic oxide dispersion strengthened alloy, J. Alloy. Comp. 536 (2012) S194–S199, https://doi.org/10.1016/j.jallcom.2011.11.055.
[22] C.L. Chen, A. Richter, R. Kögler, M. Griepentrog, P. Reinstädt, Ion-irradiation effects on dissimilar friction stir welded joints between ODS alloy and ferritic stainless steel, J. Alloy. Comp. 615 (2015) S448–S453, https://doi.org/10.1016/j.jallcom.2013.11.123.
[23] Y.H. Guo, Y.Q. Chang, J. Zhang, J.Z. Li, S. Ukai, F.R. Wan, Microstructures and ion-irradiation behaviour of friction stir welded 12Cr-ODS steel, Sci. Technol. Weld. Join. 23 (2018) 50–57, https://doi.org/10.1080/13621718.2017.1392075.
[24] B.W. Baker, Processing, Microstructure, and Material Property Relationships Following Friction Stir Welding of Oxide Dispersion Strengthened Steels, 2010, pp. 1–44.
[25] J.F. Ziegler, M.D. Ziegler, J.P. Biersack, SRIM – the stopping and range of ions in matter, Nucl. Instrum. Methods Phys. Res. Sect. B Beam Interact. Mater. Atoms 268 (2010) 1818–1823, https://doi.org/10.1016/j.nimb.2010.02.091 (2010).
[26] R.E. Stoller, M.B. Toloczko, G.S. Was, A.G. Certain, S. Dwaraknath, F.A. Garner, On the use of SRIM for computing radiation damage exposure, Nucl. Instrum. Methods Phys. Res. Sect. B Beam Interact. Mater. Atoms 310 (2013) 75–80, https://doi.org/10.1016/j.nimb.2013.05.008.
[27] T. Malis, S.C. Cheng, R.F. Egerton, EELS log-ratio technique for specimen-thickness measurement in the TEM, J. Electron. Microsc. Tech. (1988) 193–200.
[28] C.M. Parish, K.G. Field, A.G. Certain, J.P. Wharry, Application of STEM characterization for investigating radiation effects in BCC Fe-based alloys, J. Mater. Res. 30 (n.d.) 1275–1289. doi:https://doi.org/10.1557/jmr.2015.3..
[29] O.C. Hellman, J.A. Vandenbroucke, J. Rüsing, D. Isheim, D.N. Seidman, Analysis of three-dimensional atom-probe data by the proximity histogram, Microsc. Microanal. 6 (2000) 437–444, https://doi.org/10.1007/s100050010051.
[30] O.C. Hellman, J.B. Du Rivage, D.N. Seidman, Efficient sampling for three-dimensional atom probe microscopy data, Ultramicroscopy 95 (2003) 199–205, https://doi.org/10.1016/S0304-3991(02)00317-0.
[31] R.L. Klueh, D.R. Harries, High-chromium Ferritic and Martensitic Steels for Nuclear Applications, 2001, https://doi.org/10.1520/MONO3-EB.
[32] M. West, B. Jasthi, P. Hosemann, V. Sodesetti, Friction stir welding of oxide dispersion strengthened alloy MA956, in: Frict. Stir Weld. Process, vol. vol. I, 2011, pp. 33–40.
[33] J. Wang, W. Yuan, R.S. Mishra, I. Charit, Microstructure and mechanical properties of friction stir welded oxide dispersion strengthened alloy, J. Nucl. Mater. 432 (2013) 274–280, https://doi.org/10.1016/j.jnucmat.2012.08.001.
[34] S.V. Rogozhkin, A.A. Aleev, A.G. Zaluzhnyi, N.A. Iskanderov, A.A. Nikitin, P. Vladimirov, R. Lindau, A. Möslang, Atom probe tomography of nanoscaled features of oxide-dispersion-strengthened ODS Eurofer steel in the initial state and after neutron irradiation, Phys. Met. Metallogr. 113 (2012) 98–105, https://doi.org/10.1134/S0031918X12010103.
[35] S.V. Rogozhkin, A.A. Aleev, A.G. Zaluzhnyi, A.A. Nikitin, N.A. Iskandarov,

[1] The SZ 200 nm bin in Fig. 4a contained a 300 nm dispersoid leading to an abnormally higher average diameter of 90.0 nm because of the low number of dispersoids observed.

P. Vladimirov, R. Lindau, A. Möslang, Atom probe characterization of nano-scaled features in irradiated ODS Eurofer steel, J. Nucl. Mater. 409 (2011) 94–99, https://doi.org/10.1016/j.jnucmat.2010.09.021.
[36] R.S. Nelson, J.A. Hudson, D.J. Mazey, The stability of precipitates in an irradiation environment, J. Nucl. Mater. 44 (1972) 318–330.
[37] M.J. Swenson, J.P. Wharry, Nanocluster irradiation evolution in Fe-9%Cr ODS and ferritic-martensitic alloys, J. Nucl. Mater. 496 (2017) 24–40, https://doi.org/10.1016/j.jnucmat.2017.08.045.
[38] M.W. Mahoney, C.G. Rhodes, J.G. Flintoff, R.A. Spurling, W.H. Bingel, Properties of friction-stir-welded 7075 T651 aluminum, Metall. Mater. Trans. 29A (1997) 1955–1964.
[39] R.L. Klueh, J.P. Shingledecker, R.W. Swindeman, D.T. Hoelzer, Oxide dispersion-strengthened steels: a comparison of some commercial and experimental alloys, J. Nucl. Mater. 341 (2005) 103–114, https://doi.org/10.1016/j.jnucmat.2005.01.017.
[40] E. Getto, K. Sun, A.M. Monterrosa, Z. Jiao, M.J. Hackett, G.S. Was, Void swelling and microstructure evolution at very high damage level in self-ion irradiated ferritic-martensitic steels, J. Nucl. Mater. 480 (2016) 159–176, https://doi.org/10.1016/j.jnucmat.2016.08.015.
[41] D.S. Gelles, Microstructural development in reduced activation ferritic alloys irradiated to 200 dpa at 420°C, J. Nucl. Mater. 212–215 (1994) 714–719, https://doi.org/10.1016/0022-3115(94)90150-3.
[42] J.J. Kai, G.L. Kulcinski, 14 MeV nickel-ion irradiated HT-9 ferritic steel with and without helium pre-implantation, J. Nucl. Mater. 175 (1990) 227–236, https://doi.org/10.1016/0022-3115(90)90211-5.
[43] B.H. Sencer, J.R. Kennedy, J.I. Cole, S.A. Maloy, F.A. Garner, Microstructural analysis of an HT9 fuel assembly duct irradiated in FFTF to 155dpa at 443°C, J. Nucl. Mater. 393 (2009) 235–241, https://doi.org/10.1016/j.jnucmat.2009.06.010.
[44] G. Gupta, Z. Jiao, A.N. Ham, J.T. Busby, G.S. Was, Microstructural evolution of proton irradiated T91, J. Nucl. Mater. 351 (2006) 162–173, https://doi.org/10.1016/j.jnucmat.2006.02.028.
[45] J. Gan, G.S. Was, Microstructure evolution in austenitic Fe-Cr-Ni alloys irradiated with rotons: comparison with neutron-irradiated microstructures, J. Nucl. Mater. 297 (2001) 161–175, https://doi.org/10.1016/S0022-3115(01)00615-8.
[46] J. Gan, G.S. Was, R.E. Stoller, Modeling of microstructure evolution in austenitic stainless steels irradiated under light water reactor condition, J. Nucl. Mater. 299 (2001) 53–67, https://doi.org/10.1016/S0022-3115(01)00673-0.
[47] S.M. Bruemmer, E.P. Simonen, P.M. Scott, P.L. Andresen, G.S. Was, J.L. Nelson, Radiation-induced material changes and susceptibility to intergranular failure of light-water-reactor core internals, J. Nucl. Mater. 274 (1999) 299–314, https://doi.org/10.1016/S0022-3115(99)00075-6.
[48] D.L. Damcott, T.R. Allen, G.S. Was, Dependence of radiation-induced segregation on dose, temperature and alloy composition in austenitic alloys, J. Nucl. Mater. 225 (1995) 97–107, https://doi.org/10.1016/0022-3115(94)00690-3.
[49] C. Xu, In-situ Proton Irradiation Creep of FM Steel T91 © Cheng Xu, 2014.
[50] E. Getto, Effect of Friction Stir Welding and Self -Ion Irradiation on Dispersoid Evolution in Oxide Dispersion Strengthened Steel MA956 up to 25 Dpa, 2018. Mendeley Data, https://doi.org/10.17632/k5rb7vvpm8.1.
[51] C.H. Zhang, J. Jang, H.D. Cho, Y.T. Yang, Void swelling in MA956 ODS steel irradiated with 122 MeV Ne-ions at elevated temperatures, J. Nucl. Mater. 386–388 (2009) 457–461, https://doi.org/10.1016/j.jnucmat.2008.12.161.
[52] A. Kimura, H.-S. Cho, N. Toda, R. Kasada, K. Yutani, H. Kishimoto, N. Iwata, S. Ukai, M. Fujiwara, High burnup fuel cladding materials R&D for advanced nuclear systems, J. Nucl. Sci. Technol. 44 (2007) 323–328, https://doi.org/10.1080/18811248.2007.9711289.
[53] H. Kishimoto, K. Yutani, R. Kasada, O. Hashitomi, A. Kimura, Heavy-ion irradiation effects on the morphology of complex oxide particles in oxide dispersion strengthened ferritic steels, A, J. Nucl. Mater. (2007) 367–370, https://doi.org/10.1016/j.jnucmat.2007.03.149, 179–184.
[54] H. Kishimoto, R. Kasada, A. Kimura, M. Inoue, T. Okuda, F. Abe, S. Ohnuki, T. Fujisawa, Super ODS steels R&D for fuel cladding of next generation nuclear systems: ion irradiation effects at elevated temperatures, in: Proc. ICAPP 2009, Tokyo, Japan, 2009, p. 9219.
[55] M.L. Lescoat, J. Ribis, A. Gentils, O. Kaïtasov, Y. De Carlan, A. Legris, In situ TEM study of the stability of nano-oxides in ODS steels under ion-irradiation, J. Nucl. Mater. 428 (2012) 176–182, https://doi.org/10.1016/j.jnucmat.2011.12.009.
[56] J. Ribis, M.L. Lescoat, Y. De Carlan, J.M. Costantini, I. Monnet, T. Cozzika, F. Delabrouille, J. Malaplate, Stability of nano-oxides upon heavy ion irradiation of an ODS material, J. Nucl. Mater. 417 (2011) 262–265, https://doi.org/10.1016/j.jnucmat.2010.12.068.
[57] V.A. Skuratov, A.S. Sohatsky, J.H. O'Connell, K. Kornieieva, A.A. Nikitina, V.V. Uglov, J.H. Neethling, V.S. Ageev, Latent tracks of swift heavy ions in Cr23C6 and Y-Ti-O nanoparticles in ODS alloys, Nucl. Instrum. Methods Phys. Res. Sect. B Beam Interact. Mater. Atoms 374 (2016) 102–106, https://doi.org/10.1016/j.nimb.2015.08.089.
[58] C.Z. Yu, H. Oka, N. Hashimoto, S. Ohnuki, Development of damage structure in 16Cr-4Al ODS steels during electron-irradiation, J. Nucl. Mater. 417 (2011) 286–288, https://doi.org/10.1016/j.jnucmat.2011.02.037.
[59] A. Yutani, K, R. Kasada, H. Kishimoto, Kimura, Irradiation hardening and microstructure evolution of ion-irradiation ODS ferritic steels, J. ASTM Int. (JAI) 4 (2007) 323–328.
[60] H.J. Jung, D.J. Edwards, R.J. Kurtz, T. Yamamoto, Y. Wu, G.R. Odette, Structural and chemical evolution in neutron irradiated and helium-injected ferritic ODS PM2000 alloy, J. Nucl. Mater. 484 (2016) 68–80, https://doi.org/10.1016/j.jnucmat.2016.11.022.